

# Self-Field Effects on $J_C(B, T)$ Measurements of Nb–Ti Strands in High Magnetic Fields

Francis J. Ridgeon<sup>1b</sup>, Mark J. Raine<sup>1b</sup>, M’hamed Lakrimi, Adrian Thomas, Thierry Boutboul<sup>1b</sup>,  
and Damian P. Hampshire<sup>1b</sup>

**Abstract**—We have investigated the applied magnetic field, temperature, and self-field dependence of the critical current density of a Nb–Ti strand produced for the ITER poloidal field conductor. Measurements were made on a standard ITER barrel in magnetic fields from 4.0 to 8.0 T and temperatures from 3.5 to 6.0 K. We investigated the effect of self-field by changing the direction of the transport current, resulting in an inward or outward Lorentz force acting on the strand. At 4.2 K and 5 T, the difference in the measured  $J_C$  between the two Lorentz force polarities was about 1%. From this low value, we conclude that self-field effects in the Nb–Ti strand are about 40% of those expected using standard self-field calculations for fully transposed multifilamentary strands, consistent with theoretical considerations for annular filament transposition.

**Index Terms**—Critical current, finite element methods, Nb–Ti.

## I. INTRODUCTION

THE conductors in the magnets of the ITER tokamak use Nb<sub>3</sub>Sn and Nb–Ti strands to produce the magnetic fields necessary to confine the plasma. To ensure uniform production quality, reference laboratories have measured the properties of the superconducting strands in high fields. In order to standardize critical current density ( $J_C$ ) measurements, ITER has specified a barrel for  $V$ - $I$  transport measurements. This approach means one can compare data from different laboratories without explicitly considering self-fields and has led to experimental uncertainty in  $J_C$  between different institutions to be as low as 2–3% [1], [2]. However to optimize our use of superconducting strands, we need to quantify the role of self-field in these measurements given that some work in the literature suggests the self-field corrections can be as large as 6% [3], [4].

When a transport current flows in a superconducting strand, a self-field is produced that adds to the applied field to produce a net field that varies in magnitude and direction throughout the strand [5]. In this work, we only consider high field transport

Manuscript received September 19, 2017; accepted February 7, 2018. Date of publication February 21, 2018; date of current version April 3, 2018. This work was supported by the Engineering and Physical Sciences Research Council under Grant EP/L505419/1. (Corresponding author: Francis J. Ridgeon.)

F. J. Ridgeon, M. J. Raine, and D. P. Hampshire are with the Superconductivity Group, Durham University, Durham DH1 3LE, U.K. (e-mail: f.j.ridgeon@durham.ac.uk).

M. Lakrimi and A. Thomas are with Siemens plc Healthcare Sector, MR Magnet Technology, Oxford OX29 4BP, U.K.

T. Boutboul is with the ITER Department, Fusion for Energy, 08019 Barcelona, Spain.

Color versions of one or more of the figures in this paper are available online at <http://ieeexplore.ieee.org>.

Digital Object Identifier 10.1109/TASC.2018.2808370

TABLE I  
NB–Ti STRAND CHARACTERISTICS FOR ITER COILS PF1 AND PF6

Diameter of strand	$0.730 \pm 0.005$ mm
Inter annulus radius	0.130 mm
Outer annulus radius	0.310 mm
Filament diameter	$6.8 \pm 0.2$ $\mu$ m
Cu: SC ratio	Range: 1.55 to 1.75
Critical current (4.22 K, 6.4 T)	> 306 A
Twist pitch of filaments	$15 \pm 2$ mm
$n$ -value (4.22 K, peak field)	> 20

measurements where the applied field is much larger than the self-field, the critical current densities are low and the self-field is often ignored [6]–[8]. We have measured the critical current density of an ITER Nb–Ti strand as a function of field and temperature with the current flowing both clockwise and anticlockwise in the helix. These different current polarities are specified in this paper as either inward or outward Lorentz force polarities following standard notation [3], [9]–[11]. We use these data to investigate self-field effects and compare them with both computational and analytic approaches [9].

## II. EXPERIMENTAL DETAILS

### A. Strand and Barrel

A 1.6 m long strand of Nb–Ti for ITER Poloidal Field conductor was measured. The strand characteristics are listed in Table I. The nickel plating along  $\sim 200$  mm length of the strand was removed from both ends using fine grit emery paper before being wound onto a Ti–6Al–4V ITER barrel with 1 kg of tension [12]; this ensures proper strand location within the barrel groove. These barrels have helical grooves, which enable measurements in homogenous magnetic fields with voltage tap lengths of 500 mm. The strand was temporarily fixed to the barrel using socket screws to enable the nickel-free ends to be soldered to the copper end rings, after which the screws were removed. The solder provides good electrical and mechanical connection to the barrel. The helical sample has a major radius of 15.83 mm and the separation of turns was 3.18 mm.

### B. Probe Design

The strand was measured using a custom-built probe as shown in Fig. 1. The strand, heaters and thermometers were surrounded by superinsulation and located in an insulated cup. This variable-temperature environment produced good gas stability around the

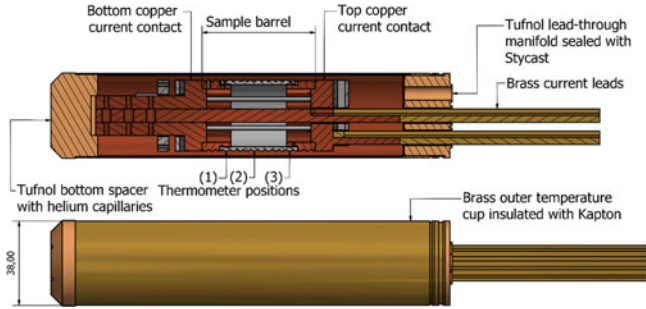


Fig. 1. Bottom end of Durham's bespoke variable temperature ITER barrel probe showing a cross section of the temperature cup with barrel and the location of the three thermometers.

strand and reduced the heat-leak from the strand region. Three independently controlled flexible Kapton heaters and three Cernox thermometers were employed to control the temperature profile within the cup. The thermometers were mounted to the barrel in dedicated grooves. Each thermometer was also thermally connected to the nearest portion of the sample using a small copper link and thermal grease. The Cernox thermometers were calibrated in zero-field commercially, and then as a function of magnetic field in-house. One thermometer was centrally positioned within the voltage tap region and the other two were mounted on either side of the voltage taps. Using standard PID feedback loops, three Lakeshore temperature controllers were used to control and maintain the temperature during the  $J_C$  measurements at temperatures above 4.2 K.

The current leads consisted of brass bars with high-temperature superconductor soldered to them in parallel. The cross-sectional area of the current leads was optimized to minimize the heat leak into the helium bath [13].

### C. Measurement Procedure

Measurements at 4.2 K were completed in a liquid helium bath at atmospheric pressure. To ensure the pressure of the helium remained close to atmospheric pressure, bubblers were used. A temperature correction associated with the liquid helium bath temperature being different to 4.2 K was then applied [1]. For the measurements made below 4.2 K, standard vapour-pressure thermometry was employed. The repeatability of the  $I_C$  measurements at 4.2 K is typically better than 0.1% and the noise in the measurements was a few nanovolts – primarily due to the Johnson noise from the room temperature section of the voltage leads.

For the measurements conducted above 4.2 K, the sample is in gas and the temperature controllers, heaters, and thermometers were used in closed-cycle loops to keep the temperature of the sample constant. At these higher temperatures, the temperature stability is the dominant source of noise.

Voltage–current ( $V$ – $I$ ) measurements were made in fields up to 8 T, using a superconducting magnet in Durham, as shown in Figs. 2 and 3. The current was ramped to  $I_C$  over 120 s for all  $V$ – $I$  measurements. Inward and outward Lorentz force polarities were measured by reversing the current direction as shown in Fig. 2.  $J_C$  were obtained at an electric field criterion ( $E_C$ ) of

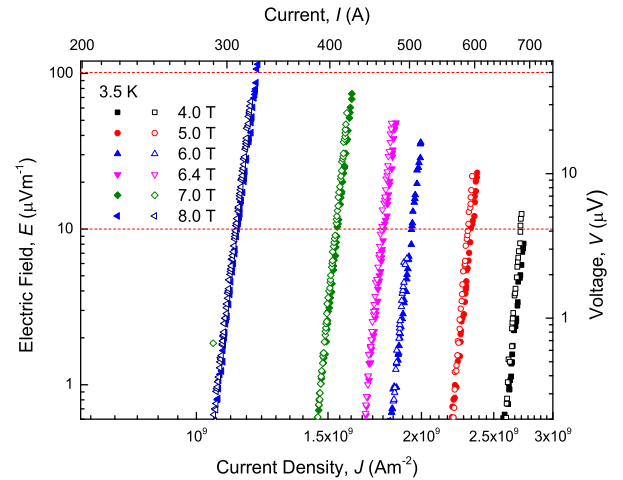


Fig. 2. Log-log plot of electric field versus current density at 3.5 K of a Nb-Ti strand measured for the two polarities of the force: inward Lorentz force (filled symbols) and outward Lorentz force (open symbols). The difference in  $J_C$  between the two orientations is typically 1% in the field range 4.0–8.0 T.

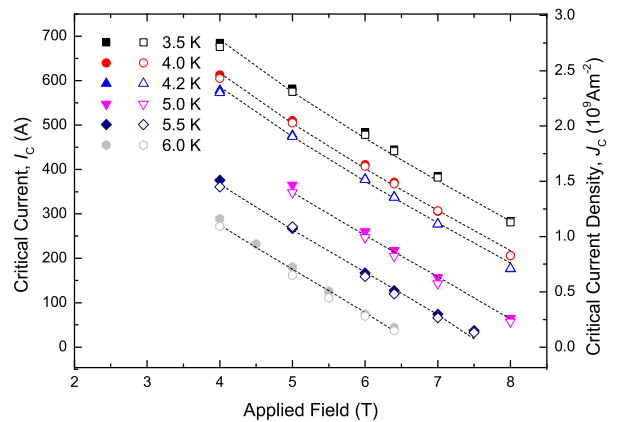


Fig. 3.  $I_C(B, T)$  of Nb-Ti strand for the two polarities of the force on the strand: inward Lorentz force (filled symbols) outward Lorentz force (open symbols). The dashed lines are a fit to all the data (both force polarities).

$10 \mu\text{Vm}^{-1}$ , and are shown in Fig. 3. The index of transition  $n$  is defined using the non-linear equation

$$E = E_C \left| \left( \frac{J}{J_C} \right)^n \right| \quad (1)$$

and was calculated over the range between 10 and  $100 \mu\text{Vm}^{-1}$ . The index of transition data are shown in Fig. 4.

### D. Reproducibility of Results

A second Nb-Ti strand was also measured at 4.2 K (not reported in detail here) in both Lorentz force polarities. The difference in the absolute values of  $I_C$  as function of field between the two strands at 5 T was less than 2% and the differences between the two Lorentz force polarities for the second strand was again about 1%, similar to that observed for the first strand. We also investigated the effect of repeated measurements in both Lorentz force polarities and found no degradation in  $J_C$ .

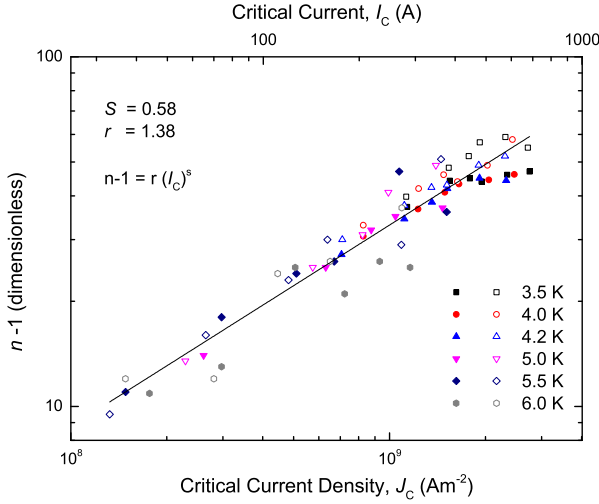


Fig. 4. Log-log plot of  $n - 1$  (where  $n$  is the index of transition) versus the critical current density for Nb-Ti at  $10 \mu\text{V} \cdot \text{m}^{-1}$  criterion. Inward Lorentz force (filled symbols) outward Lorentz force (open symbols). Data are shown at all values of field and temperature.

TABLE II

FIT PARAMETERS OF A Nb-Ti STRAND FOR BOTH LORENTZ FORCE POLARITIES

$T_{c0}$ (K)	$B_{c20}$ (T)	$C_0$ (A.T)	$\alpha$	$\beta$	$\gamma$	$\nu$	$\sigma$ (%)
9.049	14.329	14054	0.748	0.840	1.827	1.525	2.0

### III. PARAMETERIZATION OF ( $I_C$ ) AND $n$ -VALUE

We parameterised the critical current ( $I_C$ ) data using a formula for a single pinning mechanism where [4]

$$I_C = \frac{C_0}{B} b^\alpha (1 - b)^\beta (1 - t^\nu)^\gamma \quad (2)$$

where  $\alpha$ ,  $\beta$ ,  $\gamma$ ,  $\nu$  and  $C_0$  are scaling parameters,  $t = T/T_C$ ,  $b = B/B_{C2}$  and the upper critical field,  $B_{C2} = B_{C2}(0)(1 - t^\nu)$ . The results of the fitting procedure [14], with seven free parameters, are shown in Fig. 3 and the fitting parameters are listed in Table II. We parameterized the relation between the  $n$ -value and  $I_C$  using a modified power law of the form,

$$n - 1 = r(I_C)^s \quad (3)$$

where  $r$  and  $s$  only weakly depend on temperature [15] as shown in Fig. 4.

### IV. SELF-FIELD OF TRANPOSED FILAMENTS

An exact calculation of a self-field value, that characterises the difference between the spatially varying net field that each part of the superconductor experiences and the applied field, is only possible if the details of the current flow within the strand are known. In technological multifilamentary conductors, important parameters include the degree to which the filaments are transposed as they pass through the strand, the electrical coupling between the filaments as well as  $J_C$  and the index of transition,  $n$ . For straight wires, one can find some analytic solutions for the self-field of such complex materials. However

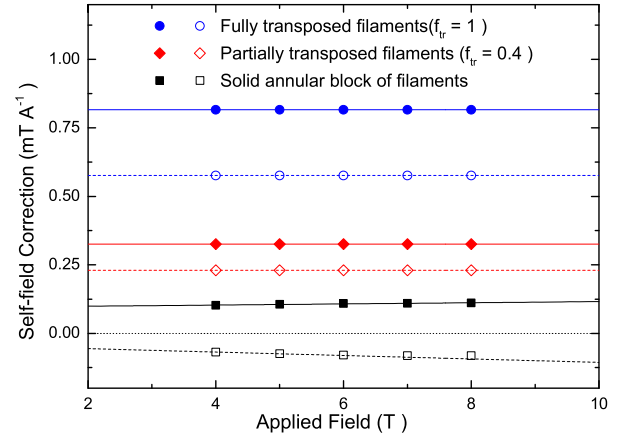


Fig. 5. The self-field correction as a function of applied field. The inward and outward Lorentz force calculations are shown for the fully transposed filaments', partially transposed filaments where  $f_{tr} = 0.4$  and a Comsol model for a solid annular block of filaments. Inward Lorentz force are open symbols and outward Lorentz force are closed symbols.

as one considers measurements on ITER barrels, with strands that have helical geometries, the calculations become extremely demanding.

#### A. Fully Transposed Filaments—Peak $B_Z$ Model

An FEA model of the self-field ( $B_{SF}$ ) for strands of various radius on an ITER barrel has been reported for each of the two Lorentz force polarities [3]. The self-field  $B_{SF}$  is given by

$$B_{SF}/I = f_{tr} \left[ \frac{\mu_0}{2\pi r} + \alpha \right] \quad (4)$$

where  $I$  is the current flowing that produces the self-field,  $r$  is the distance between the centre of the strand and the outermost superconducting filament and the constant  $\alpha = -9.0 \times 10^{-5}$  for an inward Lorentz force and  $\alpha = +1.5 \times 10^{-4}$  for an outward Lorentz force. We have added the constant  $f_{tr}$ , to characterise the degree to which the filaments are transposed and the finite  $n$ -value. It is a fractional number that is usually taken to be equal to unity in the literature (for fully transposed filaments). The model that leads to (4) equates the peak field produced at the outermost filaments of a strand to the self-field. The first term in the square brackets of (4) is associated with those regions of the strand where the peak field is parallel to the applied field. It is calculated for a straight wire and derived using Ampere's law. The second term has its origin in the helical geometry of the ITER barrel. The model effectively assumes that the filaments are fully transposed when any small part of the outermost filaments becomes normal, all the filaments are partially normal and the entire strand reaches  $J_C$ . It also assumes  $n$  is infinite so that when part of a filament reaches  $J_C$  the electric field criterion is met for the whole strand. The filaments are insulated from each other so current does not redistribute. This model is widely used, because it provides a valuable conservative (maximum) estimate of the self-field. The field-independent values of  $B_{SF}/I$  from (4) are plotted in Fig. 5 where the radius of the outermost filaments is taken from Table I and  $f_{tr} = 1$ .

### B. Partially Transposed Filaments

In practice, filaments are not fully transposed in any technological superconducting strand. During the commercial production of strands, while the strands are being drawn, they are also twisted which partially transposes the filaments and minimizes losses. This achieves an annular transposition of the filaments in the strands so that the twisted filaments remain at broadly a constant distance from the central axis of the strand. One can consider the transposed filaments in the strand to be transposed within nested cylinders. Here we consider corrections to the self-field that follow from the filaments not being fully transposed, finite  $n$ , and the vector nature of magnetic field:

**Redistribution of current density** - there is a magnetic field gradient across the strand from the self-field. In a straight wire, the self-field produced at the centre of the strand is zero. Hence the filaments at the centre of the strand, or close to the centre for a helix, carry a current density equal to that at the applied field rather than the applied field + self-field. In the limit that the self-field is small compared to the applied field and assuming the current profile is linear, the self-field is reduced from the peak-field value by a factor of  $2/3$ . More sophisticated calculations that account for the non-linear field profile within the strand give a factor of  $\sim 0.6$  [16].

**Finite  $n$**  - when  $n$  is finite and  $J \approx J_C$ , one can expect a significant length of every filament to produce an electric field similar to  $E_C$ . To account for the significant region of normal filaments, we assume that the index of transition is sufficiently low that to a first approximation we can consider the  $V-I$  characteristic to be linear near  $E_C$ . We must also consider the vectorial nature of the net magnetic field and how it affects  $J_C$ . We argue that in the ITER barrel geometry in superconducting materials such as Nb-Ti where flux pinning operates, it is the local magnitude of the net field that determines  $J_C$ . Hence the increase in  $E$ -field from those parts of the strand that experience a self-field that adds in parallel to the applied field is almost completely negated by the  $E$ -field produced in those regions where the self-field opposes the applied field. In contrast, in those regions where the self-field is orthogonal to the applied field, the self-field contributes to the net field without being negated by those regions where the self-field has opposite polarity. If we again consider the limit that the self-field is small, the self-field is reduced from the value of the peak field by a factor of  $2/\pi$ .

Hence we argue that for partial annular transposition of filaments,  $J_C$  in the strand is not reduced by a (uniform) magnetic field equal to the peak self-field produced at the surface of the strand, as occurs for the fully transposed case. We suggest that the self-field can be better described using  $f_{tr} \approx 0.6 \times 2/\pi \approx 0.4$ . In Fig. 5, the field-independent values of  $B_{SF}/I$  from (4) are plotted for partially transposed filaments where  $f_{tr} = 0.4$ .

### C. FEA for a Annular Block of Superconductor

Finally we consider the most extreme case, where the integrity of the filaments has completely broken down and there is a solid annular block of superconductor [17]. Complete redistribution of current is possible within the annulus. We have implemented a three-dimensional finite element analysis (FEA) model using

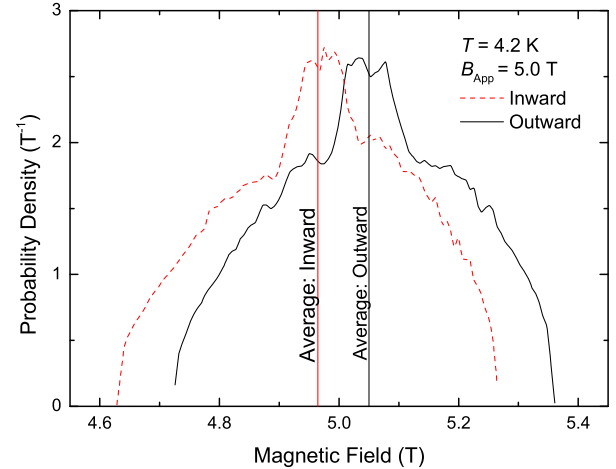


Fig. 6. Probability density function for the modulus of the net magnetic field for each of the two polarities of force on the strand: inward Lorentz force (dashed) and outward Lorentz force (solid). The distribution is calculated for the central turn of the strand in an applied field of 5 T. The difference from the applied field in the inward Lorentz force polarity is  $-35$  mT and outward  $50$  mT.

the  $H$ -formulation [18] in Comsol [19]. A 5-turn helical ITER barrel geometry was modelled. The annulus of superconductor had an internal radius of  $0.130$  mm and an outer radius of  $0.310$  mm (see Table I). The resistivity of the superconductor was defined using the  $E-J$  characteristic defined in (1) and the  $I_C$  relationship by (2). The non-superconducting modelling domain was characterised by a resistivity of  $1 \Omega\text{m}$ . The spatial distribution of the magnitude of the net magnetic field in the superconducting region is presented as a histogram of the probability density. Fig. 6 shows the probability density for the two Lorentz force polarities. There is a shift of the average to above and below the applied field and the peak field is consistent with Bordini's work [3] given by (4).

To obtain these computational data, the current density was ramped up to the average value of  $J_C$  measured experimentally at  $5$  T. The difference in the average of the field distribution (Fig. 6.) between the two polarities was  $85$  mT. This small difference in field is equivalent to an increase in  $J_C$  of  $0.8\%$  when the Lorentz force is inwards and a decrease in  $J_C$  of  $1.1\%$  when the Lorentz force is outwards. Similar detailed data to those obtained at  $5$  T in Fig. 6 were obtained over the field range  $4-8$  T for Fig. 5. At  $5$  T, the value of  $B_{SF}/I$  was calculated as follows:  $(B_{SF}/I)_{\text{Outward}} = (50 \text{ mT}) / (477 \text{ A}) = 0.10 \text{ mT} \cdot \text{A}^{-1}$  for the solid annular block of filaments data in Fig. 5.

## V. DISCUSSION AND CONCLUSION

The ITER barrel geometry is an accepted standard and self-field correction terms have been widely applied to data in the literature [20]–[24]. Our high field measurements of the difference in  $I_C$  for the two Lorentz force polarities can be compared to those predicted by (4) which together with (2) gives for  $\Delta I_C = I_{C\text{In}} - I_{C\text{Out}}$

$$\Delta I_C / I_C \approx f_{tr} \left( \frac{\partial I_C}{\partial B} \right)_{I_c} [-\alpha_{In} + \alpha_{Out}], \quad (5)$$

where  $(\partial I_C / \partial B)_{I_c} = 100 \text{ A T}^{-1}$  is obtained from (2). Equation (5) has helical geometry terms alone since to first order the straight wire contribution to  $\Delta I_C$ , is zero. Using the experimental result  $\Delta I_C / I_C \approx 1\%$  at 5 T, (5) gives  $f_{tr} \approx 0.42$ . This value is consistent with annular transposition of filaments discussed in Section IV and provides a *prima facie* case that the effect of self-fields in the Nb-Ti strand are significantly lower than predicted by the model for fully transposed strands. In particular, the self-field correction from (4) for our measurements at 5 T should be  $\sim 100$  mT, rather than the value of  $\sim 250$  mT calculated for a fully transposed strand.

Extended measurements of  $J_C$  with  $B$  and  $T$  in the literature have used a wide variety of different designs for barrels [20]. Future work will consider non-standard barrels with more realistic multifilamentary composite strands.

#### ACKNOWLEDGMENT

The authors would like to thank Steve Lishman in the Durham mechanical workshop. Associated materials are on the Durham Research Online website: <http://dro.dur.ac.uk/>. The Nb-Ti strand was produced by ChMP (Glasov, Russia) for ITER PF conductor.

#### REFERENCES

- [1] I. Pong *et al.*, "Worldwide benchmarking of ITER internal Tin Nb<sub>3</sub>Sn and NbTi strands test facilities," *IEEE Trans. Appl. Supercond.*, vol. 22, no. 3, Jun. 2012, Art. no. 4802606.
- [2] C. Zhou, D. Bessette, A. Devred, G. Romano, and A. Vostner, "The scaling parameterization of ITER superconducting Nb-Ti strands throughout worldwide production," *IEEE Trans. Appl. Supercond.*, vol. 26, no. 4, Jun. 2016, Art. no. 6000204.
- [3] B. Bordini, "Self-field correction in critical current measurements of superconducting wires tested on ITER VAMAS barrels," Eur. Org. Nucl. Res., Genève, Switzerland, Internal Note EDMS 1105765, 2010.
- [4] L. Bottura, "A practical fit for the critical surface of NbTi," *IEEE Trans. Appl. Supercond.*, vol. 10, no. 1, pp. 1054–1057, Mar. 2000.
- [5] M. N. Wilson, *Superconducting Magnets*. Oxford, U.K.: Oxford Univ. Press, 1986.
- [6] W. M. de Rapper, B. Bordini, S. le Naour, L. Bottura, and H. H. J. ten Kate, "Critical current in high- $J_c$  Nb<sub>3</sub>Sn Rutherford cables affected substantially by the direction of the applied magnetic field," *IEEE Trans. Appl. Supercond.*, vol. 22, no. 3, Jun. 2012, Art. no. 6001704.
- [7] M. Garber, A. K. Ghosh, and W. B. Sampson, "The effect of self field on the critical current determination of multifilamentary superconductors," *IEEE Trans. Magn.*, vol. 25, no. 2, pp. 1940–1944, Mar. 1989.
- [8] L. D. Cooley, P. S. Chang, and A. K. Ghosh, "Magnetization, RRR and stability of Nb<sub>3</sub>Sn strands with high sub-element number," *IEEE Trans. Appl. Supercond.*, vol. 17, no. 2, pp. 2706–2709, Jun. 2007.
- [9] L. F. Goodrich and A. N. Srivastava, "II-3: Critical current measurement methods: Quantitative evaluation," *Cryogenics*, vol. 35, pp. S19–S23, 1995.
- [10] J. W. Ekin, *Experimental Techniques for Low-Temperature Measurements*. New York, NY, USA: Oxford Univ. Press, 2007, p. 296.
- [11] J. W. Ekin, "Effect of transverse compressive stress on the critical current and upper critical field of Nb<sub>3</sub>Sn," *J. Appl. Phys.*, vol. 62, pp. 4829–4834, 1987.
- [12] *Superconductivity—Part 1: Critical Current Measurement—DC Critical Current of Nb-Ti Composite Superconductors*, IEC Standard 61788-1:2006, 2006.
- [13] P. Sunwong, J. S. Higgins, and D. P. Hampshire, "Probes for investigating the effect of magnetic field, field orientation, temperature and strain on the critical current density of anisotropic high-temperature superconducting tapes in a split-pair 15 T horizontal magnet," *Rev. Sci. Instrum.*, vol. 85, 2014, Art. no. 065111.
- [14] I. Pong *et al.*, "Current sharing temperature of NbTi SULTAN samples compared to prediction using a single pinning mechanism parametrization for NbTi strand," *Supercond. Sci. Technol.*, vol. 25, 2012, Art. no. 054011.
- [15] D. M. J. Taylor and D. P. Hampshire, "Relationship between the  $n$ -value and critical current in Nb<sub>3</sub>Sn superconducting wires exhibiting intrinsic and extrinsic behaviour," *Supercond. Sci. Technol.*, vol. 18, pp. S297–S302, 2005.
- [16] F. J. Ridgeon, M. J. Raine, M. Lakrimi, A. Thomas, T. Boutboul, and D. P. Hampshire, "The self-field of NbTi strands for the ITER poloidal fields," unpublished.
- [17] J. W. Ekin, "Current transfer in multifilamentary superconductors. I. Theory," *J. Appl. Phys.*, vol. 49, pp. 3406–3409, 1978.
- [18] M. Zhang and T. A. Coombs, "3D modeling of high- $T_c$  superconductors by finite element software," *Supercond. Sci. Technol.*, vol. 25, 2012, Art. no. 015009.
- [19] *Finite-Element Software Package COMSOL Multiphysics, 5.1 ed.*, COMSOL Inc., Stockholm, Sweden, 2015. [Online]. Available: <https://www.comsol.com/release-history>
- [20] N. Salunin *et al.*, "The  $J_C(B, T)$  characterization of commercial NbTi strands for ITER PF 1&6 coils," *IEEE Trans. Appl. Supercond.*, vol. 22, no. 3, Jun. 2012, Art. no. 4804604.
- [21] Y. V. Karasev, *et al.*, " $J_C(B, T)$  characterization of commercial NbTi strands for the ITER poloidal field coils by transport and magnetization methods," *IEEE Trans. Appl. Supercond.*, vol. 23, no. 3, Jun. 2013, Art. no. 6001304.
- [22] A. Godeke, *et al.*, "A review of conductor performance for the LARP high-gradient quadrupole magnets," *Supercond. Sci. Technol.*, vol. 26, Sep. 2013, Art. no. 095015.
- [23] Y. V. Karasev, *et al.*, "Study of the temperature and field dependence of the critical currents in Nb-Ti strands for the ITER poloidal field magnet system," *IEEE Trans. Appl. Supercond.*, vol. 24, no. 3, Jun. 2014, Art. no. 6000204.
- [24] J. W. Ekin, N. Cheggour, L. F. Goodrich, J. Splett, B. Bordini, and D. Richter, "Unified scaling law for flux pinning in practical superconductors: II. Parameter testing, scaling constants, and the extrapolative scaling expression," *Supercond. Sci. Technol.*, vol. 29, 2016, Art. no. 123002.